

Stealth multiboson signals

J. A. Aguilar-Saavedra

Departamento de Física Teórica y del Cosmos, Universidad de Granada,
E-18071 Granada, Spain

Abstract

We introduce the ‘stealth bosons’ S , light boosted particles with a decay $S \rightarrow AA \rightarrow q\bar{q}q\bar{q}$ into two daughter bosons A , which subsequently decay into four quarks that are reconstructed as a single fat jet. Variables that measure the two-prong structure of fat jets, which are used for diboson resonance searches in hadronic or semi-leptonic final states, classify the jets produced in stealth boson decays as QCD-like — actually, for these variables they may seem more background-like than the QCD background itself. The number of tracks in those jets can also be much higher than for the fat jets arising from the hadronic decay of boosted W and Z bosons. Heavy resonances decaying into two such stealth bosons, or one plus a W/Z boson, could offer an explanation for the recurrent small excesses found in hadronic diboson resonance searches near an invariant mass of 2 TeV.

1 Introduction

Small excesses around an invariant mass of 2 TeV appear in no less than five different searches for diboson resonances decaying hadronically, performed by the ATLAS and CMS Collaborations at the Large Hadron Collider (LHC), and with energies of 8 and 13 TeV. Although none of these excesses is statistically significant on its own, it is difficult to regard them as a mere coincidence. Yet, their interpretation as a background shaping or a new physics signal is difficult too.

The largest excess, of 3.4σ , was found by the ATLAS Collaboration in a search using the full Run 1 dataset at 8 TeV [1], and sparked a great interest. The excess appeared in the (non-independent) samples tagged as WW , WZ and ZZ , but it was largest for the WZ event selection. Before, a mild excess had been found by the CMS Collaboration [2], though the maximum significance was below 2σ , and located at slightly smaller invariant masses. The first ATLAS analysis of Run 2 data with 3.2 fb^{-1} at 13 TeV [3], did not show any hint of an excess with the nominal WZ event selection but relaxing the boson tagging criteria for fat jets a third bump appeared, again around 2 TeV, in one of the control distributions (the dijet invariant mass distribution without an upper cut on the number of tracks per jet). The significance of this bump was later estimated to be of

2.4σ [4]. When the analysis was updated with a luminosity of 15.5 fb^{-1} [5], a bump at 2 TeV appeared also with the nominal WZ selection, with a significance around 2σ . The fifth 2 TeV bump has appeared recently in the CMS search with the full 2016 dataset, using a luminosity of 35.9 fb^{-1} [6]. Its significance is around 2σ . No excess at this mass was observed in earlier analyses with 2.6 fb^{-1} [7] and 12.9 fb^{-1} [8].

Before addressing other explanations, it is worthwhile mentioning that two different studies [4, 9] have pointed out using Monte Carlo simulation that a small knee appears in the QCD dijet invariant mass distribution around $m_{JJ} = 1.7 \text{ TeV}$ when the jet mass and subjettiness criteria used for boson tagging in the ATLAS searches are applied. This knee arises because the boson tagging affects differently the quark and gluon jets. But the predicted knee, a slight decrease in the slope of the dijet invariant mass distribution, is by no means a bump around 2 TeV as observed in data. Moreover, it is questionable that the same background shaping, if any, would appear at two centre-of-mass energies in two experiments that use different jet radii, filtering and tagging criteria for the analyses. And, of course, it is also expected that the ATLAS and CMS Collaborations will have checked with Monte Carlo simulations that the boson tagging criteria applied do not produce a distortion in the smoothly falling background, before releasing their results. We will then discard the possibility of a significant background shaping in the following.

Regarding new physics interpretations, it was early pointed out [10] that the 3.4σ ATLAS excess at 8 TeV was unlikely to result from a VV diboson resonance, $V = W, Z$, as the searches in the semi-leptonic final states [11, 12] did not exhibit any deviation from the standard model (SM) prediction. The proposal in ref. [10] was of a VVX triboson resonance, that is, a resonance R undergoing a cascade decay $R \rightarrow VY \rightarrow VVX$ yielding two SM bosons plus an additional particle X , with Y being an intermediate resonance. The presence of an extra particle X would dramatically decrease the efficiency of such a signal in the searches in semileptonic modes, as it was later confirmed in ref. [4] with a more detailed analysis. The reason is that the mentioned Run 1 searches in semileptonic modes, as well as the more recent ones with Run 2 data [13–17], are highly optimised for the kinematics of diboson resonances produced back-to-back in the transverse plane. Moreover, the event selection criteria often veto the presence of extra particles near the decay products of the boson with leptonic decay, which obviously dampens the efficiency for such a signal. As an alternative explanation for the lack of a positive signal in the semileptonic decay channels, it was proposed [18] that the two hadronically decaying ‘bosons’ identified as two fat jets are not actually massive SM gauge bosons but smuons of similar mass, decaying into two quarks via R -parity violating interactions, and the heavy 2 TeV resonance is a sneutrino. That is, the observed ‘bosons’ simply do not have leptonic decay modes.

In ref. [19] it has been shown that a wide bump on a smoothly-falling distribution that cannot be predicted from simulations is quite difficult to detect in narrow resonance searches: the bump can easily be absorbed in the background normalisation. This is indeed the case for diboson resonance searches in hadronic final states, where the background is obtained from a fit to data in the signal region, assuming some smooth functional form. This feature may partially explain why excesses are not seen in the searches that have a smaller dataset. Still, current new physics interpretations are undermined by an apparent inconsistency among the size of the excesses. For example, in ref. [4] a variety of triboson signals that accommodated the ATLAS Run 1 excess was examined in order to give predictions for other analyses, in particular for the hadronic Run 2 CMS search with 2.6 fb^{-1} . The predictions were compatible with the null experimental result but in the latest dataset [6], with a luminosity 13 times higher, a larger excess should have appeared. The same reckoning is expected to apply to a simple signal such as the one proposed in ref. [18], with two particles from a resonance decay, each decaying into a quark pair. A possible solution to this puzzle is suggested by a comparison of the different hadronic searches, focusing not on the number of observed events, but rather on the *expected* QCD background at dijet invariant masses around 2 TeV, and its dependence on the boson tagging criteria [20]:

- CMS analyses use a subjettness ratio τ_{21} [21] to quantify the likeliness that the jets have a two-prong structure. For the so-defined ‘high purity’ (HP) jets, the criterion has strengthened from $\tau_{21} \leq 0.5$ in the Run 1 analysis [2], to $\tau_{21} \leq 0.45$ [7], $\tau_{21} \leq 0.4$ [8], and $\tau_{21} \leq 0.35$ [6], as the dataset has increased. To give an example, the expected background near 2 TeV for the high purity dijet sample is similar in the latest analysis with 35.9 fb^{-1} and the previous one with 12.9 fb^{-1} , clearly showing that the requirements on jets are tighter.
- For the ATLAS analyses the comparison between Run 1 and Run 2 is not easy, because in Run 1 a cut $\sqrt{y} \geq 0.45$ on the y variable [22] measuring the subjet momentum balance is used, whereas in Run 2 it is replaced by a momentum-dependent cut on the so-called D_2 function [23]. Nevertheless, by assuming a naive parton luminosity scaling of the expected background around 2 TeV, it is seen that the boson tagging criteria for the Run 2 nominal selection [3] are around one order of magnitude stronger.

Getting together the above arguments, namely (i) the persistence of the 2 TeV bumps, (ii) the unlikely possibility of a background shaping, (iii) the apparent inconsistency of the size of the bumps, an obvious question arises: *May it be possible to have new physics signals giving fat jets whose substructure is background-like?* If this were the case, those

signals would be more and more suppressed as the jet tagging requirements are tightened, and we might have an explanation for that apparent inconsistency. As we show in this paper, the answer is affirmative. The cascade decay of a very boosted particle S with a mass $M_S \sim M_Z, M_W$ into two lighter particles A that subsequently decay each into two quarks,

$$S \rightarrow A A \rightarrow q \bar{q} q \bar{q}, \quad (1)$$

gives a single fat jet with a mass consistent with the W and Z masses. (The particles S and A can be for instance a new scalar H_1^0 and pseudo-scalar A^0 , respectively, in models with an extended scalar sector.) And, depending on the A mass M_A , the fat jet originated in the decay of S may seem more background-like than the QCD background itself, when one considers jet subjettiness measures such as τ_{21} or D_2 . Therefore, it is appropriate to denote these S bosons as ‘stealth bosons’.

This striking observation will be the starting point of our analysis. In section 2 we consider the diboson-like decay of a heavy resonance R into two such stealth bosons, $R \rightarrow SS$, and compare the resulting variables with those for a true diboson resonance $Z' \rightarrow WW$. There, our statement that those signals can be more background-like than the QCD background will be apparent. In section 3 we study a diboson-like decay $R \rightarrow VS$ of a resonance into a SM boson and a stealth boson, and in section 4 a triboson-like cascade decay $R \rightarrow VY \rightarrow VVS$, with Y an intermediate resonance. As an example of these cascade decays, as well as for the Monte Carlo simulations, we use the multiboson signals that arise in left-right models [24], but our results will not be limited to such specific examples. We finally discuss our results in section 5. Although the novel ‘stealth boson’ signatures introduced in this work are motivated by the 2 TeV excesses, we point out that they are interesting on their own. Such signatures are relatively hard to spot over the QCD background with the standard diboson resonance searches, and therefore they are so far quite unexplored.

2 Diboson-like $R \rightarrow SS$ decays

The $R \rightarrow SS$ decay depicted in figure 1 actually yields a quadriboson final state, but will resemble a diboson resonance if S is much lighter than R . Such a signal can arise in left-right models if CP is violated in the scalar sector, so that the CP-odd and CP-even states mix, or in simpler Z' extensions of the SM with additional scalars. We take in our simulations $R = Z'$ with $M_R = 2$ TeV, $S = H_1^0$ with $M_S = 100$ GeV and consider $A = A^0 \rightarrow b\bar{b}$ decays in ‘high mass’ and ‘low mass’ benchmarks, with $M_A = 40$ and 20 GeV, respectively. The relevant Lagrangian is implemented in FEYNRULES [25] in order

to generate events with MADGRAPH5_AMC@NLO [26] using the universal Feynrules output [27]. Event generation is followed by hadronisation and parton showering with PYTHIA 8 [28]. The detector response is simulated with DELPHES 3.4 [29], and for the jet reconstruction and analysis FASTJET 3.2 [30] is used.

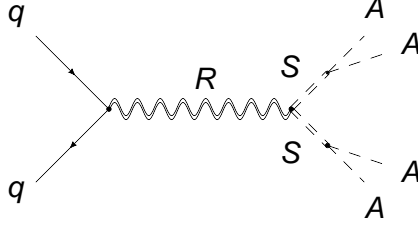


Figure 1: Sample diagram for a $R \rightarrow SS$ signal.

The CMS hadronic searches use jets with a large radius $R = 0.8$ reconstructed with the anti- k_T algorithm [31], referred to as AK8 jets, as vector boson candidates. A jet-pruning algorithm is performed on the AK8 jets, which starts from all original constituents of the jet and discards soft recombinations after each step of the Cambridge-Aachen algorithm [32]. The most recent analysis selects events with two jets J_1, J_2 (ordered by transverse momentum) having pseudorapidities $|\eta| \leq 2.5$, pseudorapidity difference $|\Delta\eta| \leq 1.3$, transverse momentum $p_T \geq 200$ GeV and invariant mass $m_{JJ} \geq 1.05$ TeV. These kinematical criteria, which are usually referred to as ‘topological selection’, are quite similar for previous CMS analyses. Jets are considered as W -tagged if they satisfy a condition on τ_{21} specified below and their mass is in the range 65 – 85 GeV, and Z -tagged if their mass is in the range 85 – 105 GeV.

The N -subjettiness ratio variable $\tau_{21} = \tau_2/\tau_1$ is used to enrich the sample with di-boson candidates. A low-purity (LP) category is defined for jets with $\tau_{21} \leq 0.75$, and a HP category with $\tau_{21} \leq 0.45, 0.3, 0.35$, depending on the particular analysis considered. Events are classified as HP if they have two HP jets, and LP if they have one HP and one LP jet. The τ_{21} distributions for the leading and subleading jets for a $Z' \rightarrow WW$ sample with $M_{Z'} = 2$ TeV are shown in figure 2, for jets within the mass window 65 – 105 GeV and fulfilling the above acceptance criteria. The distributions have a shape similar to the one obtained by the CMS Collaboration [6], also with a maximum in the 0.25 – 0.3 bin. This, in particular, shows that the τ_{21} variable is adequately modeled by the fast simulation. In contrast, the distributions for $R \rightarrow SS$ lean towards higher values of τ_{21} and are background-like, especially for $M_A = 40$ GeV. (For the QCD background the maximum of the distribution obtained by the CMS Collaboration, not shown in our plot, is located at the 0.5 – 0.55 bin.)

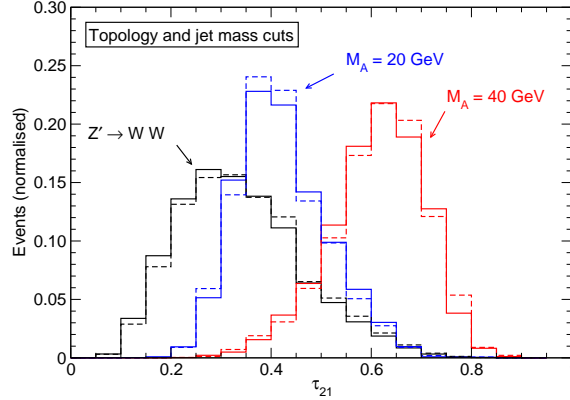


Figure 2: N -subjettiness ratio τ_{21} for $R \rightarrow SS$ and $Z' \rightarrow WW$ signals. Solid (dashed) lines correspond to the leading (subleading) jet.

The background-like behaviour of stealth bosons is reflected in a significant efficiency drop as the τ_{21} cut is tightened. For example, for the HP WZ selection (two HP jets, one W -tagged and the other Z -tagged) the efficiencies for the WW diboson and SS stealth diboson signals are reduced as follows,¹

$$\begin{aligned} WW : & & 0.068 \rightarrow 0.031 & (\times 0.45), \\ M_A = 20 \text{ GeV} : & & 0.035 \rightarrow 0.0035 & (\times 0.1), \end{aligned}$$

when strengthening the cut from $\tau_{21} \leq 0.45$ to $\tau_{21} \leq 0.35$. (For $M_A = 40$ GeV the efficiency is essentially zero already for $\tau_{21} \leq 0.45$.) This is precisely the ‘anomalous’ behaviour anticipated for this type of signals in the introduction.

The jet mass distributions are also of interest. They are shown, after topological selection but before the boson tagging, in the top panels of figure 3, for the leading and subleading jets. While for the lower mass benchmark the boson masses are adequately reconstructed, this is not the case for the higher mass, though a sizeable fraction of events still fall within the W or Z tagging mass windows. We also point out that the dijet invariant mass distribution before boson tagging is wider than for a true diboson resonance, and peaks at lower invariant masses, as shown in the bottom left panel of figure 3. After boson tagging (right panel), the distribution for $M_A = 20$ GeV is still wide while for $M_A = 40$ GeV the simulated signal does not pass the boson tagging.

We now study the features of the $R \rightarrow SS$ signals under the ATLAS Run 2 analyses.

¹For the benchmark $Z' \rightarrow WW$ diboson signal the efficiency is larger with the WW selection. Still, we give our results for the WZ selection for better comparison with previous work, and also because we have assumed that the new boson S is heavier than the Z boson. In any case, the overall efficiency for WW , WZ or ZZ mass tagging for the signals does not affect our arguments.

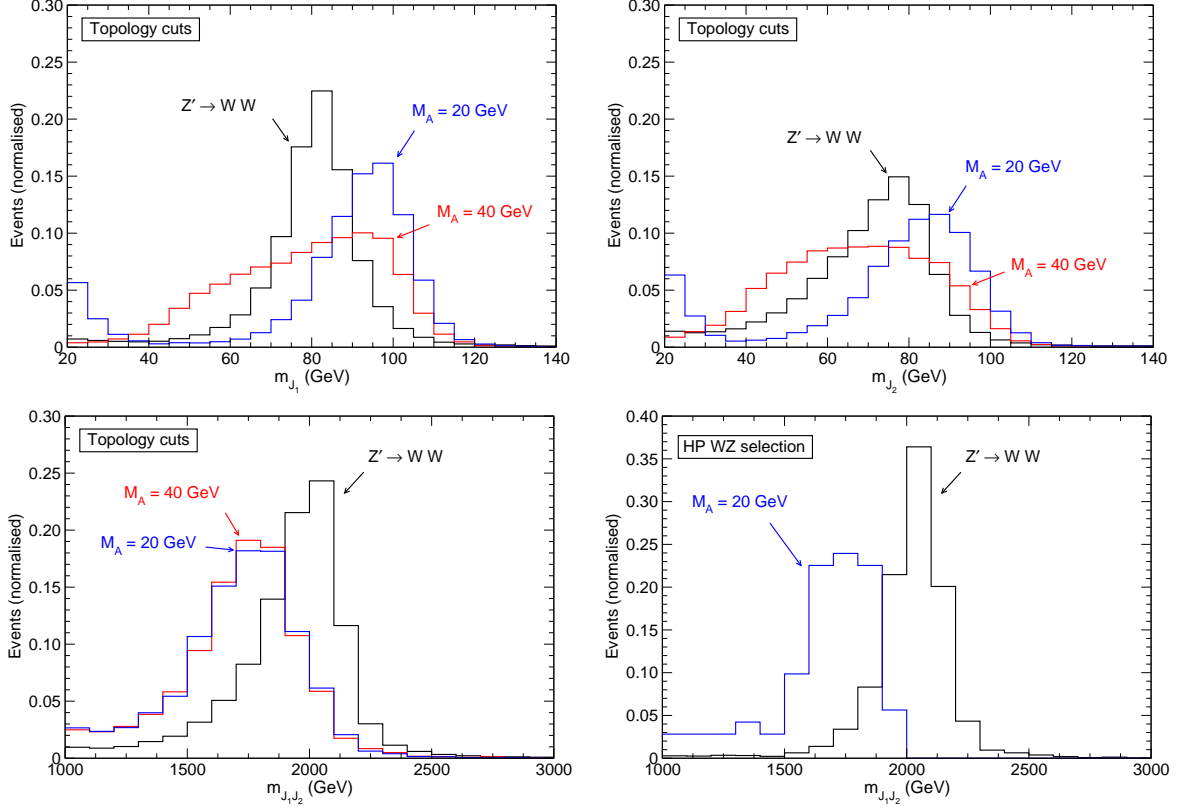


Figure 3: Jet and dijet mass distributions for $R \rightarrow SS$ and $Z' \rightarrow WW$ signals for the CMS analysis.

The ATLAS Collaboration uses wider jets with radius $R = 1.0$, reconstructed with the anti- k_T algorithm. Fat jets are trimmed by re-clustering the large- R jet constituents using the anti- k_T algorithm with $R = 0.2$ and dropping any of the sub-jets with p_T less than 5% of the original jet p_T . As topological selection, events must contain two fat jets, the leading one with $p_T \geq 450$ GeV and the subleading one with $p_T \geq 200$ GeV, both within $|\eta| \leq 2.0$ and with a small rapidity separation $|\Delta y_{12}| \leq 1.2$. The dijet invariant mass m_{JJ} must be larger than 1 TeV. At variance with the CMS analyses, a transverse momentum balance cut is here introduced, $(p_{T1} - p_{T2})/(p_{T1} + p_{T2}) < 0.15$.

The $D_2^{(\beta=1)}$ variable, abbreviated throughout this paper as D_2 , is used to characterise the two-prong substructure, and a p_T -dependent upper cut is imposed [33], approximately $D_2 \leq 1 + 0.8(p_T - 300)/1200$ with p_T in GeV. An upper cut $N_{\text{trk}} < 30$ is also placed on the number of tracks with $p_T \geq 0.5$ GeV in the ungroomed jets, pointing to the primary vertex. Jets satisfying both criteria are tagged as W or Z candidates if their mass is within an interval of ± 15 GeV around the expected resonance peak. Notice that a jet can simultaneously be tagged as W and Z , therefore the WW , WZ and ZZ samples are not

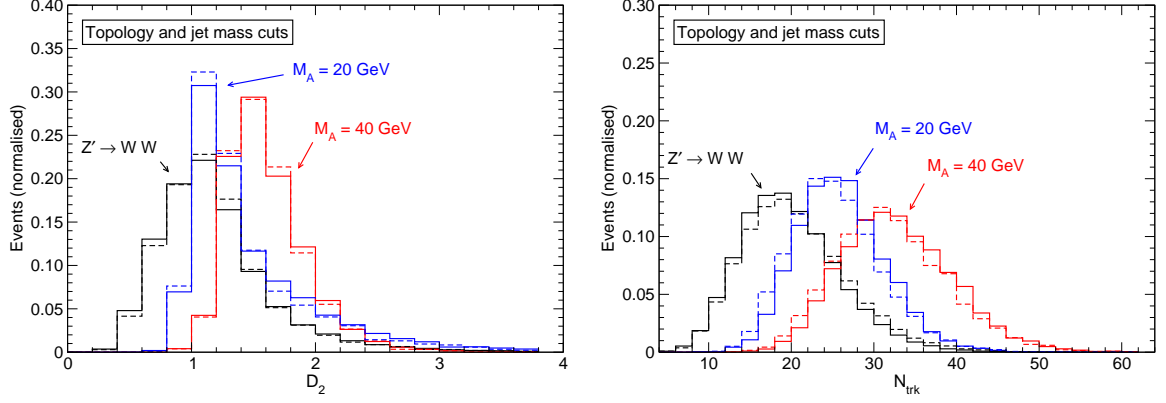


Figure 4: D_2 variable (left) and number of tracks (right) for $R \rightarrow SS$ and $Z' \rightarrow WW$ signals. Solid (dashed) lines correspond to the leading (subleading) jet.

disjoint.

We present the D_2 distribution for the different signals after topology and mass cuts in figure 4 (left). For $Z' \rightarrow WW$ the distribution is similar to the one obtained by the ATLAS Collaboration [34], slightly shifted to smaller D_2 values. For $R \rightarrow SS$ the distributions are background-like, especially for $M_A = 40$ GeV. This is expected from what we have observed for the analogous τ_{21} variable used by the CMS Collaboration. The application of the D_2 requirement on both jets has a 50% efficiency for the $Z' \rightarrow WW$ diboson signal, 24% for $R \rightarrow SS$ in the low-mass benchmark and only 6% in the high-mass benchmark.

The distribution of the number of tracks N_{trk} for the ungroomed jets is shown in the right panel of figure 4. For a true diboson signal $Z' \rightarrow WW$, our results are close to the ones obtained by the ATLAS Collaboration, with a slightly smaller number of tracks predicted by our simulation. For $R \rightarrow SS$ with $M_A = 20$ GeV, the distribution has a maximum at the 25–26 bin, close to the maximum of the QCD background in the ATLAS simulation (not shown in our plot). For $M_A = 40$ GeV the signals have many more tracks than the background itself. For the WZ selection, the requirement $N_{\text{trk}} < 30$ reduces the signals as

WW :	$0.18 \rightarrow 0.16$	$(\times 0.89)$,
$M_A = 20$ GeV :	$0.10 \rightarrow 0.065$	$(\times 0.65)$,
$M_A = 40$ GeV :	$0.017 \rightarrow 0.0024$	$(\times 0.14)$.

Therefore, a requirement of a small number of tracks leads to an additional suppression of this type of signals, besides the one from the D_2 tagging.

The wider $R = 1.0$ jets and filtering algorithm used by the ATLAS Collaboration allow for a better jet mass determination for stealth bosons than with the CMS analyses. We

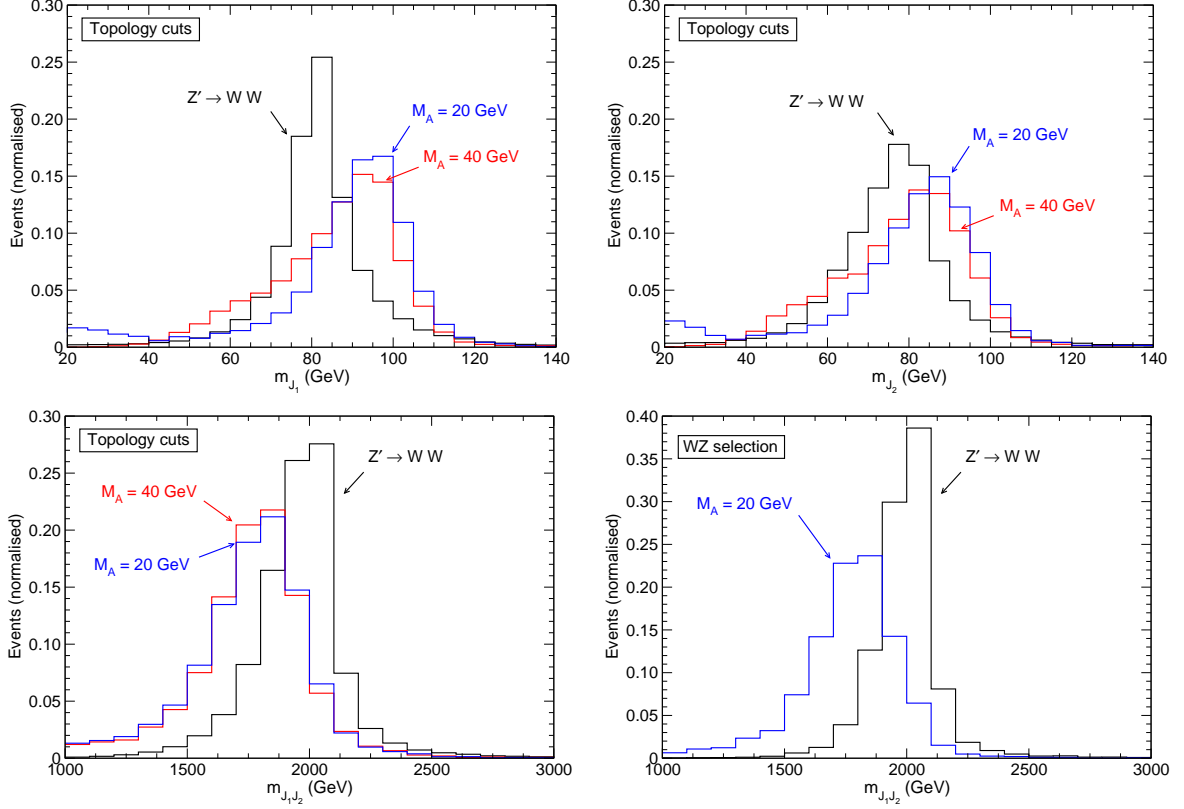


Figure 5: Jet and dijet mass distributions for $R \rightarrow SS$ and $Z' \rightarrow WW$ signals for the ATLAS analysis

show in figure 5 (top) the masses of the leading and subleading jet after the topological selection. The shapes are less peaked than for true bosons but still the distributions are quite similar, with obvious differences due to the input value $M_S = 100$ GeV used that is larger than the W mass. The dijet mass distributions on the bottom panels are very wide, and similar after topology cuts only (left) and with the full WZ tagging (right). In the latter case the corresponding plot for $M_A = 40$ GeV is not shown because the signal is tiny.

To conclude this section, we compare in table 1 the efficiencies for the WZ selection in the ATLAS Run 1 [1] and Run 2 [5] searches. The results are indeed eloquent. While for a true diboson signal the efficiency of the ATLAS Run 2 event selection is larger than in Run 1, for the $R \rightarrow SS$ signals it is noticeably smaller — which may have motivated the disappearance of the excess in the first Run 2 result with the nominal selection, if it is due to a signal of this type. Of course, the precise numbers vary with M_A , but the trend is the correct one. The comparison of these figures with the efficiency for the CMS selection is not meaningful because for CMS analyses the jet mass windows are narrower,

	Run 1	Run 2
WW	0.14	0.16
$M_A = 20 \text{ GeV}$	0.10	0.065
$M_A = 40 \text{ GeV}$	3.6×10^{-3}	2.4×10^{-3}

Table 1: Efficiencies of $R \rightarrow SS$ and $Z' \rightarrow WW$ signals for the WZ selection in ATLAS hadronic diboson searches.

and the events in the WW , WZ and WW categories, which are disjoint, are combined to obtain the limits on a potential signal.

3 Diboson-like $R \rightarrow VS$ decays

We repeat the same procedure of the previous section for a $R \rightarrow VS$ decay such as the one depicted in figure 6, which yields a triboson final state but with a diboson-like topology. Such a signal can originate for example in left-right models from the decay $W' \rightarrow WH_1^0$,

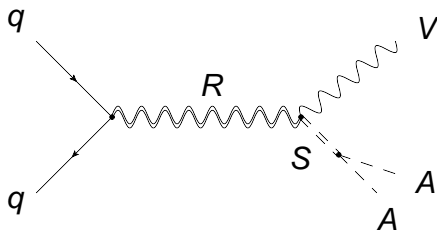


Figure 6: Sample diagram for a $R \rightarrow VS$ signal.

with subsequent $H_1^0 \rightarrow A^0 A^0$ decay [24], or also from $Z' \rightarrow ZH_1^0$. We will consider the former process, with $S = H_1^0$, $A = A^0$ and the same parameters as in section 2. The results, for what concerns the hadronic diboson searches, would be analogous for a signal of the latter type with a Z boson in the final state.

For the CMS analysis the τ_{21} distributions for the leading and subleading jets are separately shown in figure 7. These distributions are a combination of the ones for the W and S bosons in figure 2, but they are obviously correlated: always one of the two jets, the one corresponding to S , has a very large τ_{21} . For this reason, it is illustrative to quantify the efficiency drop when one changes the τ_{21} cut from 0.45 to 0.35,

$$\begin{aligned}
M_A = 20 \text{ GeV} : & \quad 0.068 \rightarrow 0.013 & (\times 0.2), \\
M_A = 40 \text{ GeV} : & \quad 4.3 \times 10^{-3} \rightarrow 5.5 \times 10^{-4} & (\times 0.13).
\end{aligned}$$

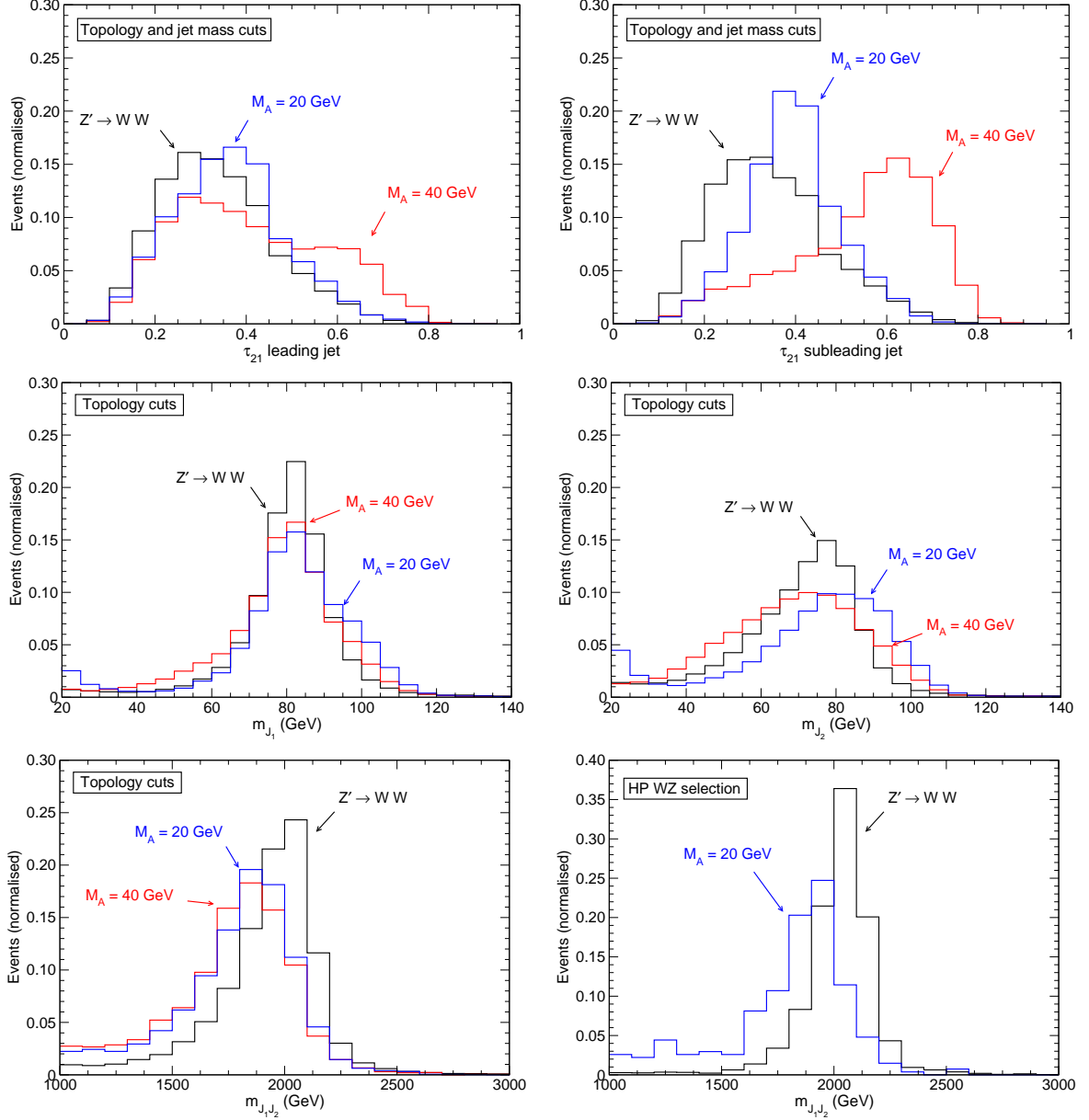


Figure 7: Distributions for the $R \rightarrow VS$ and $Z' \rightarrow WW$ signals in the CMS analysis. Top: N -subjettiness ratio τ_{21} ; middle: jet mass distributions; bottom: dijet mass distributions.

The masses of the leading and subleading jets are also shown in figure 7. The distributions are narrower than for a $R \rightarrow SS$ decay, as expected because one of the decay products is a massive SM boson. The dijet invariant mass distributions are very wide, peaking at invariant masses slightly lower than the resonance mass. For $M_A = 20$ GeV the distribution after boson tagging is slightly sharper, comparable to a true diboson resonance, while for $M_A = 40$ GeV most of the signal does not pass the boson tagging selection and is not shown.

For the ATLAS Run 2 analyses the D_2 and N_{trk} boson tagging variables are shown in figure 8. For the leading jet the distributions are similar for the three signals, indicating that the leading jet in $R \rightarrow VS$ is the SM vector boson in most cases. The D_2 tagging requirement on both jets has an efficiency of 0.35 and 0.18 for $M_A = 20$ and 40 GeV, respectively, larger than for the $R \rightarrow SS$ signal. Here it is also interesting to see the effect of the $N_{\text{trk}} < 30$ cut, which reduces the signal efficiencies for the WZ selection as follows,

$$\begin{aligned} M_A = 20 \text{ GeV} : & \quad 0.13 \rightarrow 0.096 & (\times 0.74), \\ M_A = 40 \text{ GeV} : & \quad 0.055 \rightarrow 0.020 & (\times 0.36). \end{aligned}$$

For this type of signals an upper cut on the number of tracks may be counterproductive too, especially for heavier A .

Besides the jet substructure differences found, the topology and jet mass of the $R \rightarrow VS$ signal is rather similar to a true diboson resonance, as it can be seen by comparing the rest of distributions presented in figure 8, namely the masses of the leading and subleading jet after the topological selection, the dijet invariant mass after topological selection and also with the final WZ tagging. The distributions are less peaked than for a true diboson but still they are fairly similar. Finally, we collect in table 2 the efficiencies for the full WZ tagging in the ATLAS Run 1 / Run 2 analyses. At variance with the results shown in the previous section, the efficiencies for both ATLAS analyses are similar, but slightly smaller in Run 2. Such a signal might also accommodate the size of the excesses observed in the different searches.

	Run 1	Run 2
$M_A = 20 \text{ GeV}$	0.11	0.096
$M_A = 40 \text{ GeV}$	0.022	0.020

Table 2: Efficiencies of $R \rightarrow VS$ signals for the WZ selection in ATLAS hadronic diboson searches.

4 Triboson-like $R \rightarrow VVS$ decays

As our third example we consider a cascade decay $R \rightarrow VY \rightarrow VVS$, with subsequent decay $S \rightarrow AA$, as depicted in figure 9. This is a quadriboson signal but with a triboson-like topology. There are two crucial differences with the previously seen resonance decays. First, there are already two SM bosons in the final state, which produce fat jets with a higher boson tagging efficiency. Second, the invariant mass of the two selected jets does

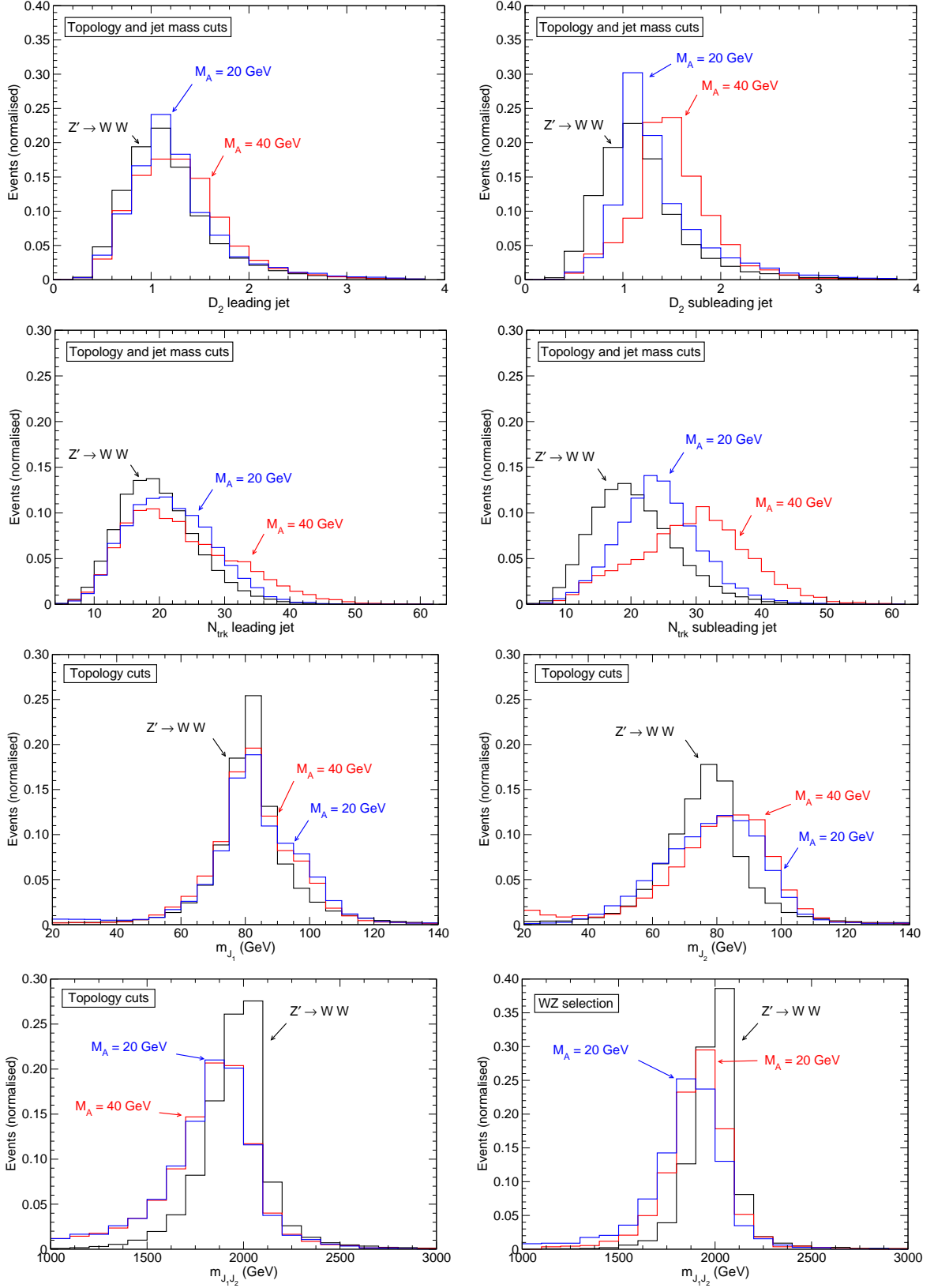


Figure 8: Distributions for the $R \rightarrow VS$ and $Z' \rightarrow WW$ signals in the ATLAS analysis. Top: D_2 variable; second row: number of tracks; third row: jet mass; bottom: dijet invariant mass.

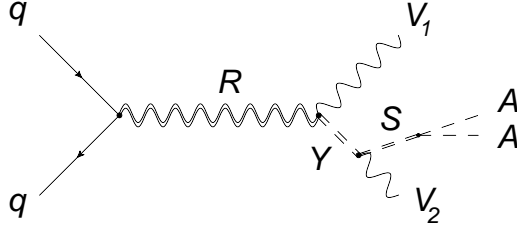


Figure 9: Sample diagram for a $R \rightarrow V_1 Y \rightarrow V_1 V_2 S$ signal.

not concentrate at a maximum near or below the resonance mass, but instead the dijet invariant mass distributions are broader [10]. An example of this cascade decay chain is $W' \rightarrow ZH^\pm \rightarrow ZW^\pm H_1^0$ in left-right models [24]. This is the signal used in our simulations, with $Y = H^\pm$ with $M_Y = 500$ GeV, $S = H_1^0$, $A = A^0 \rightarrow b\bar{b}$.

For this signal we collect the relevant distributions for the CMS analysis in figure 10. The τ_{21} distribution for the leading jet is quite close to the one for a $Z' \rightarrow WW$ diboson signal, while there are some differences for the subleading jet. (This indicates that the leading jet is the Z boson from the heavy resonance decay in most cases.) The efficiency for τ_{21} and mass tagging does not change as dramatically as for the previous $R \rightarrow SS$ and $R \rightarrow VS$ examples,

$$\begin{aligned} M_A = 20 \text{ GeV} : & \quad 0.13 \rightarrow 0.056 & (\times 0.43), \\ M_A = 40 \text{ GeV} : & \quad 0.088 \rightarrow 0.041 & (\times 0.47), \end{aligned}$$

that is, it decreases by nearly the same amount as for a $Z' \rightarrow WW$ signal. The jet mass distributions are not very different from a diboson resonance either. Note that here the leading jet mass concentrates around M_Z , as corresponds to the simulated signal. Sharp differences are found in the dijet invariant mass distributions in the bottom panels of figure 10. The m_{JJ} distribution does not display any resonance-like structure before the boson tagging (left) and a wide bump, similar to the ones found for triboson signals in ref. [4], appears after boson tagging.

The distributions for the ATLAS Run 2 analyses are given in figure 11. The D_2 variable for the leading and subleading jets in the top panels follows quite similar distributions as for the benchmark $Z' \rightarrow WW$ signal, and the efficiency for the D_2 cut in both jets is 0.4 for $M_A = 20$ GeV and 0.33 for $M_A = 40$ GeV, closer to the value of 0.5 for a WW signal. The number of tracks per jet is slightly higher, as it can be seen from the plots in the second row. For the WZ selection, the $N_{\text{trk}} < 30$ cut reduces the signal efficiencies as

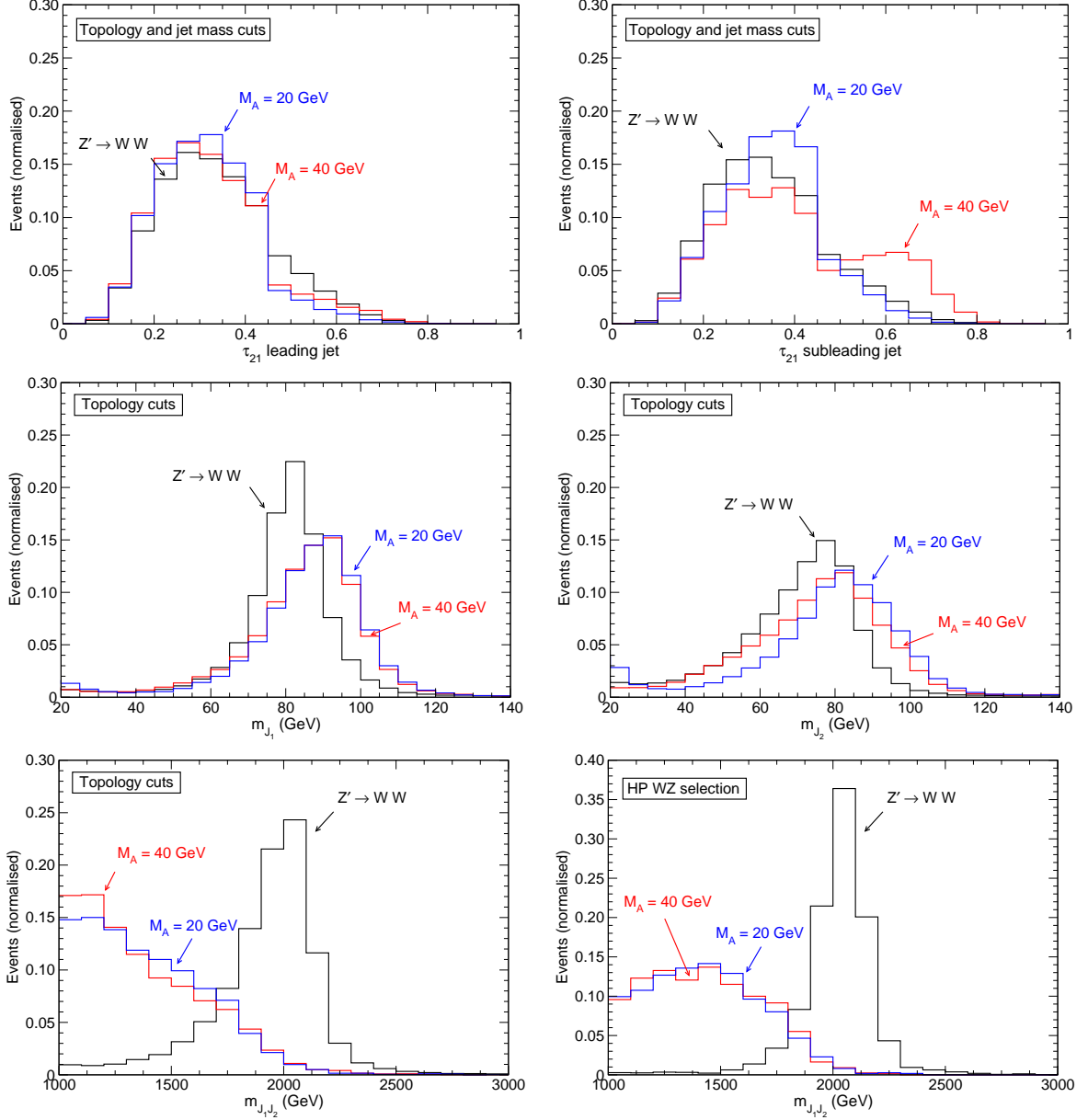


Figure 10: Distributions for the $R \rightarrow VVS$ and $Z' \rightarrow WW$ signals in the CMS analysis. Top: N -subjettiness ratio τ_{21} ; middle: jet mass distributions; bottom: dijet mass distributions.

follows,

$$\begin{aligned}
 M_A = 20 \text{ GeV} : & \quad 0.082 \rightarrow 0.063 & (\times 0.77), \\
 M_A = 40 \text{ GeV} : & \quad 0.058 \rightarrow 0.042 & (\times 0.72).
 \end{aligned}$$

That is, the signal suppression is higher than for a true diboson signal but not dramatic. The jet mass distributions are relatively narrow and similar to the CMS analysis, and the

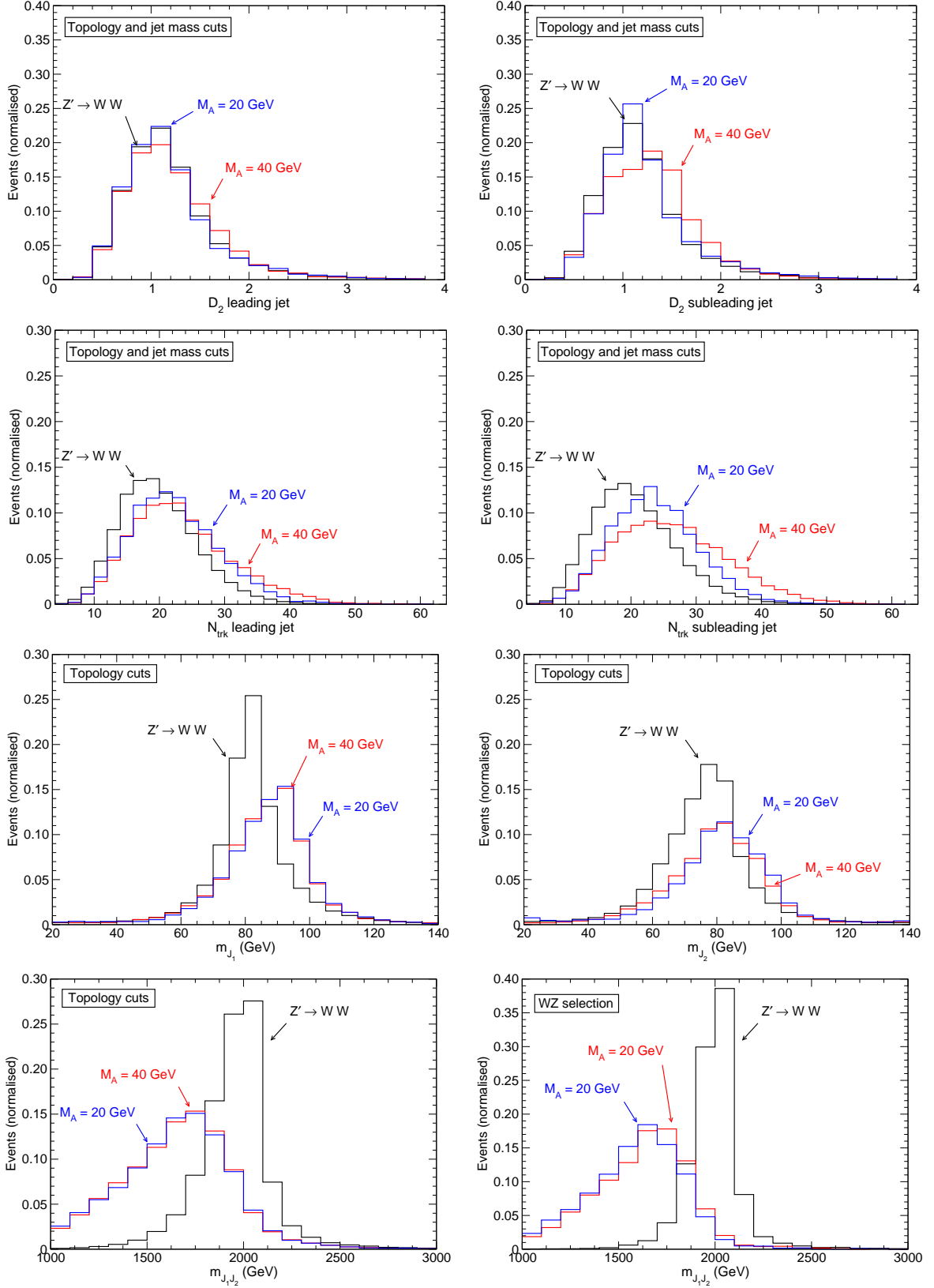


Figure 11: Distributions for the $R \rightarrow VVS$ and $Z' \rightarrow WW$ signals in the ATLAS analysis. Top: D_2 variable; second row: number of tracks; third row: jet mass; bottom: dijet invariant mass.

dijet invariant mass distributions do not display a peak either, even after the application of the full WZ selection. This contrasts with the behaviour of true triboson signals, for which the invariant mass distribution of the two leading jets is shaped to a peak by the application of topological and boson tagging cuts [4,10]. The comparison of the efficiencies for ATLAS Run 1 and Run 2 analyses is given in table 3. They are slightly smaller in Run 2. Overall, we find that except for some efficiency decrease when the boson tagging requirements are tightened, the VVS signals behave in much the same way as the triboson signals studied before [4].

	Run 1	Run 2
$M_A = 20 \text{ GeV}$	0.074	0.063
$M_A = 40 \text{ GeV}$	0.050	0.042

Table 3: Efficiencies of $R \rightarrow VS$ signals for the WZ selection in ATLAS hadronic diboson searches.

5 Discussion

New physics interpretations of the ATLAS Run 1 diboson excess [1] can explain the absence of signals in the semileptonic channels, either because the signal is due to a VVX triboson resonance [10] or by assuming a particle with a mass close to M_W, M_Z and decaying into $q\bar{q}$ only [18]. (New physics interpretations as a diboson resonance were early disfavoured, and have been already excluded with the first Run 2 results.) Nevertheless, the main difficulty for these proposals is posed by the most recent ATLAS and CMS searches in the hadronic channels, which again exhibit some mild excesses at the same mass, but with sizes that are apparently inconsistent. Even taking into account that, as shown in ref. [19], part of the excess may be absorbed by the normalisation of the background if statistics are small, one would expect more significant excesses in the large samples collected in Run 2.

The ‘stealth bosons’ S introduced in this paper, which decay into four quarks that merge into a single fat jet, can successfully address these apparent inconsistencies. We have found that:

1. For the $R \rightarrow SS$ and $R \rightarrow VS$ signals the boson tagging efficiency for CMS analyses drops when the cut on the τ_{21} variable, used to measure the two-prong structure of the jets, is tightened. This may explain why the latest CMS analysis with 35.9

fb^{-1} [6] does not observe a much larger excess, and the previous one with 12.9 fb^{-1} [8] had a small deviation at the 1σ level.

2. For $R \rightarrow SS$ especially, and to some extent for $R \rightarrow VS$ and $R \rightarrow VVS$ too, the efficiency for the ATLAS Run 2 event selection is smaller than at Run 1, explaining why the Run 2 excess with 15.5 fb^{-1} [5] was of only 2σ , and with 3.2 fb^{-1} the deviation was at the 1σ level [3].
3. The upper cut on the number of tracks N_{trk} for ungroomed jets applied by the ATLAS Collaboration washes out a $R \rightarrow SS$ signal. The suppression is milder for $R \rightarrow VS$ and $R \rightarrow VVS$. This might explain why the dijet mass distribution without this cut exhibits a bump already with 3.2 fb^{-1} [3], as already pointed out [4, 24].

We have not addressed the visibility of these signals in the semileptonic diboson searches. Still, a few comments are in order. For $R \rightarrow SS$ signals the leptonic decays are absent, and for $R \rightarrow VVS$ we expect a similar efficiency suppression for the semileptonic searches as it was found for VVX triboson signals in ref. [4]. The only potentially visible leptonic signatures may arise for $R \rightarrow VS$ signals, which deserve a detailed study. For these final states the efficiency is generally expected to be smaller than for true diboson resonances, and with the particularity that the signal may pollute the control regions where the SM backgrounds from $t\bar{t}$, W/Z plus jets, etc. are normalised, causing an unpredictable effect in the signal regions. This is quite a delicate study and falls out of the scope of this paper. Other signatures from the production of the light states S and A depend on their coupling to SM fermions — note that they do not couple to SM gauge bosons — and it is likely that with adequate model building the potential constraints can be evaded.

Our results are very encouraging and may provide guidance for new hadronic diboson searches, in order to better investigate the nature of the recurrent excesses found. In particular, (i) additional signal regions, or even new analyses with looser requirements on τ_{21} and D_2 should be also considered; (ii) relaxing the mass window for at least one of the bosons would allow to investigate signals with non-SM bosons; (iii) different N -subjettiness criteria might be investigated, in order to measure the three- and four-prong structure of fat jets; (iv) triboson resonance searches should also be performed. And regarding standard diboson searches, if the diboson candidate samples after event selection increase with the growing LHC luminosity — thus avoiding a further tightening of the boson tagging — a sufficiently large sample will be collected to investigate the profile and characteristics of the deviations.

Acknowledgements

I thank J.C. Collins and S. Lombardo for previous collaboration. This work has been supported by MINECO Projects FPA 2016-78220-C3-1-P and FPA 2013-47836-C3-2-P (including ERDF), and by Junta de Andalucía Project FQM-101.

References

- [1] G. Aad *et al.* [ATLAS Collaboration], arXiv:1506.00962 [hep-ex].
- [2] V. Khachatryan *et al.* [CMS Collaboration], JHEP **1408** (2014) 173 [arXiv:1405.1994 [hep-ex]].
- [3] ATLAS collaboration, ATLAS-CONF-2015-073.
- [4] J. A. Aguilar-Saavedra, J. H. Collins and S. Lombardo, JHEP **1609** (2016) 050 [arXiv:1607.08911 [hep-ph]].
- [5] ATLAS collaboration, ATLAS-CONF-2016-055.
- [6] CMS Collaboration, CMS-PAS-B2G-17-001.
- [7] CMS Collaboration, CMS-PAS-EXO-15-002.
- [8] CMS Collaboration, CMS-PAS-B2G-16-021.
- [9] A. Martin and T. S. Roy, Phys. Rev. D **94** (2016) no.1, 014003 [arXiv:1604.05728 [hep-ph]].
- [10] J. A. Aguilar-Saavedra, JHEP **1510** (2015) 099 [arXiv:1506.06739 [hep-ph]].
- [11] G. Aad *et al.* [ATLAS Collaboration], Eur. Phys. J. C **75** (2015) 5, 209 [arXiv:1503.04677 [hep-ex]].
- [12] V. Khachatryan *et al.* [CMS Collaboration], JHEP **1408** (2014) 174 [arXiv:1405.3447 [hep-ex]].
- [13] ATLAS collaboration, ATLAS-CONF-2016-082.
- [14] ATLAS collaboration, ATLAS-CONF-2016-062.
- [15] CMS Collaboration, CMS-PAS-B2G-16-022.

- [16] CMS Collaboration, CMS-PAS-HIG-16-034.
- [17] CMS Collaboration, CMS-PAS-B2G-16-020.
- [18] B. C. Allanach, P. S. B. Dev and K. Sakurai, Phys. Rev. D **93** (2016) no.3, 035010 [arXiv:1511.01483 [hep-ph]].
- [19] J. A. Aguilar-Saavedra, JHEP **1705** (2017) 066 [arXiv:1703.06153 [hep-ph]].
- [20] J. A. Aguilar-Saavedra, talk at the Spanish LHC network meeting, Madrid, 8-9 May 2017, <https://indico.cern.ch/event/611567/>
- [21] J. Thaler and K. Van Tilburg, JHEP **1103** (2011) 015 [arXiv:1011.2268 [hep-ph]].
- [22] J. M. Butterworth, A. R. Davison, M. Rubin and G. P. Salam, Phys. Rev. Lett. **100** (2008) 242001 [arXiv:0802.2470 [hep-ph]].
- [23] A. J. Larkoski, I. Moulton and D. Neill, JHEP **1412** (2014) 009 [arXiv:1409.6298 [hep-ph]].
- [24] J. A. Aguilar-Saavedra and F. R. Joaquim, JHEP **1601** (2016) 183 [arXiv:1512.00396 [hep-ph]].
- [25] A. Alloul, N. D. Christensen, C. Degrande, C. Duhr and B. Fuks, Comput. Phys. Commun. **185** (2014) 2250 [arXiv:1310.1921 [hep-ph]].
- [26] J. Alwall *et al.*, JHEP **1407** (2014) 079 [arXiv:1405.0301 [hep-ph]].
- [27] C. Degrande, C. Duhr, B. Fuks, D. Grellscheid, O. Mattelaer and T. Reiter, Comput. Phys. Commun. **183** (2012) 1201 [arXiv:1108.2040 [hep-ph]].
- [28] T. Sjostrand, S. Mrenna and P. Z. Skands, Comput. Phys. Commun. **178** (2008) 852 [arXiv:0710.3820 [hep-ph]].
- [29] J. de Favereau *et al.* [DELPHES 3 Collaboration], JHEP **1402** (2014) 057 [arXiv:1307.6346 [hep-ex]].
- [30] M. Cacciari, G. P. Salam and G. Soyez, Eur. Phys. J. C **72** (2012) 1896 [arXiv:1111.6097 [hep-ph]].
- [31] M. Cacciari, G. P. Salam and G. Soyez, JHEP **04** (2008) 063 [arXiv:0802.1189 [hep-ph]].
- [32] S. Catani, Y. L. Dokshitzer, M. H. Seymour and B. R. Webber, Nucl. Phys. B **406** (1993) 187.

[33] ATLAS collaboration, ATL-PHYS-PUB-2015-033.

[34] Additional material at <https://atlas.web.cern.ch/Atlas/GROUPS/PHYSICS/PAPERS/EXOT-2016-01/>